2.1 MICROSTRUCTURE CHARACTERIZATION OF NEUTRON IRRADIATED AND HELIUM INJECTED PM2000, 14YW, AND MODIFIED F82H ALLOYS

— B. Yao, D. J. Edwards, R. J. Kurtz (Pacific Northwest National Laboratory), G. R. Odette, T. Yamamoto (University of California Santa Barbara)

OBJECTIVE

To characterize the microstructure of reduced activation ferritic/martensitic steel/oxide dispersion strengthened (RAFM/ODS) alloys irradiated to a helium concentration/neutron dose of 1230 appm He and 21.2 dpa at 500°C in the High Flux Isotope Reactor (HFIR) at Oak Ridge National Laboratory.

SUMMARY

Two ODS alloys and one RAFM steel (i.e., PM2000, 14YW, and modified F82H, respectively) with an adjacent 4.7 μm thick NiAl layer bond were neutron irradiated to a dose of 21.2 dpa at 500°C. An *in situ* ^{59}Ni(n, α) reaction in the NiAl layer produces high-energy He ions, which are implanted into the alloys. This report summaries initial TEM characterization results. The PM2000 contains a high density of small (< 2 nm) He bubbles in the matrix, while at the interface of Y-rich particles large voids are found. Both 14YW and modified F82H (F82H-mod) exhibit a large number of voids. The voids in the 14YW sample coexist with small Y_2O_3 particles typically less than 10 nm. Dislocation loops in all three samples were also quantified. A higher density of <100>{100} than that of ½<111>{111} loops was observed. The loop size in PM2000 is bigger than those in the other samples.

PROGRESS AND STATUS

Introduction

Due to their excellent high-temperature mechanical properties and high swelling-resistance, reduced activation ferritic/martensitic (RAFM) steels and oxide-dispersed strengthened (ODS) alloys are promising first-wall and blanket structural materials for future nuclear fusion reactors [1,2]. The extremely severe environment induced by the fusion reaction requires materials able to withstand high dose neutron irradiation, high concentrations of transmutation produced He, high temperatures, large stresses, and potentially corrosive coolants [3]. A high concentration of He can degrade material performance. As He has a negligible solubility in metals and alloys, it readily combines with irradiation-induced and thermal vacancies to form He-vacancy complexes and eventually He bubbles in both the matrix and on interfaces such as martensite lath boundaries, grain boundaries, and secondary-phase particle-matrix interfaces [4]. A high density of small bubbles may impede dislocation movement and contribute to irradiation hardening. Furthermore, He bubbles, if allowed to reach a critical size, can transition into unstable growing voids, which can cause significant swelling [5]. High concentrations of He, either in large cavities/voids or small He bubbles at grain boundaries are undesirable because high-temperature tensile and creep properties may be degraded along with fracture toughness. One strategy to control He is by introducing a high density of bubble nucleation sites (e.g. dislocations, nano-oxides) to trap the He gas atoms in the matrix, to some extent screening the grain boundaries [1]. Besides He bubbles and voids, the formation of dislocation loops is another concern. It has been reported that sessile <100> dislocation loops are strong obstacles

to dislocation movement [6]. Both small gas bubbles and dislocation loops are microstructural features contributing to irradiation hardening.

As fusion reactors are not available to test material performance, alternate approaches are needed to simulate the anticipated irradiation conditions. Recently, a novel approach, the *in situ* He injection (IHSI) technique, has been developed to examine the effects of simultaneous neutron irradiation and He injection on microstructural evolution of candidate alloys [7]. The IHSI technique has been described in detail elsewhere [7]. In this report, we present transmission electron microscopy (TEM) characterization results of neutron irradiated and He injected RAFM/ODS alloys. Two ODS alloys and one RAFM steel (i.e., PM2000, 14YW, and modified F82H, respectively) with 4.7 μm thick NiAl layer bonded or adjacent to a sample surface were neutron irradiated to a dose of 21.2 dpa at 500°C. The He concentration in regions near the NiAl coating is calculated to be about 1230 appm. Focused ion beam (FIB) methods were used to prepare cross-sectional foils for TEM study. Features such as He bubbles and voids, dislocation loops, secondary-phases, and nano-oxides were characterized.

Specimen Preparation and TEM Characterization Methods

The compositions of the RAFM/ODS alloys examined are listed in Table 1. Among them, samples PM2000 and 14YW are ODS alloys fabricated through powder metallurgical procedures. Details of the material fabrication were described in Ref. 7. Sample F82H-mod is a RAFM alloy processed by conventional steel metallurgy. Before the irradiation, a 20% cold work was applied to the F82H-mod specimen to generate a high dislocation density. All samples were neutron irradiated to a dose of 21.2 dpa at 500°C. The thickness of NiAl is 4.7 μm, which gives a He concentration of about 1230 appm in the alloy matrix extending to a depth of ~ 6 μm away from the NiAl coating.

Table 1. Composition of examined RAFM/ODS alloys

Alloy	Composition (wt.%) with Fe balance									
	Cr	Ti	$Y(Y_2O_3)$	C	Al	W	Mn	Si	Ni	V
PM2000	19.00	0.5	0.5	-	5.5		-	-	-	-
14YW	14.00	-	0.25	-	-	3.00	-	-	-	-
F82H-mod	8.16	<0.005	-	0.097	-	1.98	0.13	0.10	0.01	0.20

Cross-sectional TEM samples of irradiated specimens were prepared by a FIB (FEI Quanta 3D). Foils were roughly cleaned with 2 keV Ga^+ ion beam at ±4° tilt angles to remove artifacts. The final cleaning was conducted using low-energy Ar^+ ion milling (Fischione Model 1040 NanoMill). A reference specimen, well annealed unirradiated pure Fe (99.99%), was used to determine FIB/nanomilling procedures to give artifact-free TEM foils. It was found that the reference foil after cleaning with the parameters listed in Table 2 does not exhibit any visible bubbles at under-focused TEM imaging conditions, and there is no diffraction contrast similar to irradiated-induced clusters or dislocation loops under bright-field two-beam condition and weak-beam dark-field imaging conditions. All TEM specimens of irradiated alloys were cleaned using the same procedure.

The TEM characterization was performed using a JEOL 2010F microscope working at 200 keV. The thickness of TEM samples was determined through convergent-beam electron diffraction (CBED). Sample compositions were confirmed using Energy Dispersive X-ray Spectroscopy (EDXS). Bright-field TEM images of He bubbles and voids were acquired at an under-focus of 750 nm. The measured bubble size corresponds to the inner-diameter of the first dark Fresnel ring. Based on our previous TEM imaging simulations, this measured value is about 87% of the actual bubble size at a defocus of 750 nm [8]. The dislocation loop was imaged using multiple diffraction vectors at two-beam conditions. A novel approach based on both crystallographic projection and *g.b=0* contrast has been adopted for the loop analysis [9]. It is noted that loops smaller than 4 nm cannot be differentiated from nano-oxides based on diffraction contrast at two-beam conditions. These small loops were excluded during loop quantification, although the ODS samples do contain a high density of such ultrafine contrast.

Table 2. Nanomilling cleaning procedures for artifact-free TEM samples.

Step	High tension (eV)	Time (min)	Beam current (nA)	Milling size (μm)	Tilt angle (°)	Temperature (°C)
1	1800	45				
2	900	45	150	40 × 20	± 10	-165
3	500	30				

RESULTS AND DISCUSSION

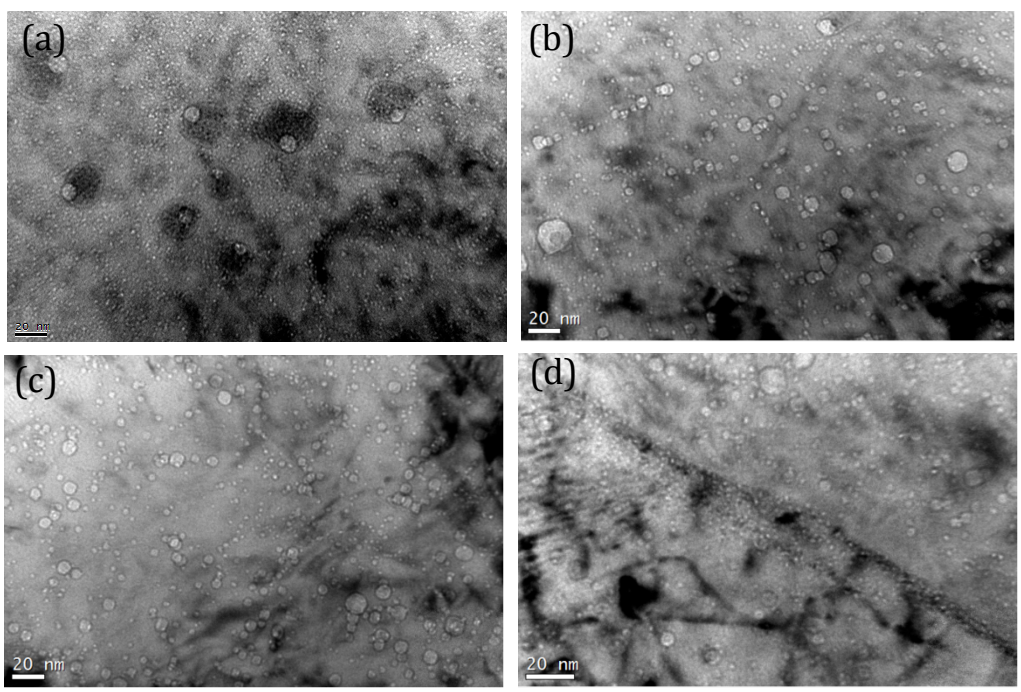

Fig. 1. TEM micrographs of He bubbles and voids in (a) PM2000, (b) 14YW, (c) F82H-mod, and (d) at a 14YW lath boundary.

Table 3. Size and density of He bubble/voids and dislocation loops in three alloys.

Alloy	He bubbles/voids		<100> dislocation loops		½<111> dislocation loops	
	size (nm)	density (m^{-3})	size (nm)	density (m^{-3})	size (nm)	density (m^{-3})
PM2000	Interface: 9.2 Matrix: 1.7	Interface: 9.3×10^{20} Matrix: 3.2×10^{23}	30.0±9.8	3.7×10^{21}	18.5±5.3	1.3×10^{21}
14YW	2.8	1.7×10^{23}	16.6±8.2	3.8×10^{21}	10.6±3.1	6.1×10^{20}
F82H-mod	3.7	6.9×10^{22}	18.6±5.3	3.0×10^{21}	Large: 38 Small: 13	1.6×10^{20}

Fig. 1 presents an overview of He bubble and voids distributed within three samples. The measured bubble sizes and densities are summarized in Table 3. The bubbles in the matrix of PM2000 (Fig. 1a) have an average size less than 2 nm, and the size distribution (not shown) is very narrow. At the interface of Y-rich particles, however, large voids up to 10 nm are found. Samples 14YW and F82H-mod contain both small He bubbles and large voids, as shown in Figs. 1b and 1c, respectively. The faceted planes of voids in both samples were identified to be mainly {100}. A few voids with {110} faceted planes were also observed. Despite a large fraction of voids distributed in the matrix, the lath boundaries were consistently decorated with a high density of small He bubbles less than 2 nm. One example of sample 14YW is shown in Fig. 1(d).

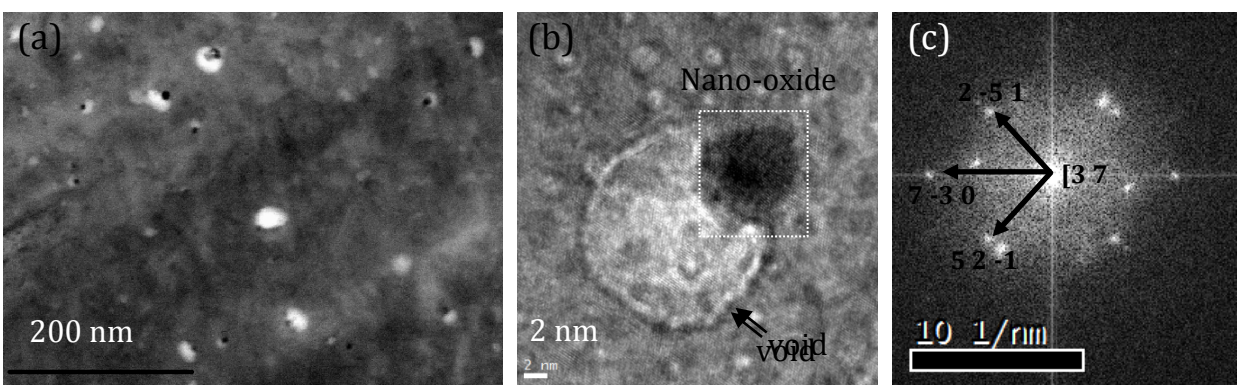

Fig. 2. TEM characterization of void-associated nano-particles in sample 14YW, (a) bright field image, (b) lattice image, and (c) FFT of the region in (b). The particle can be identified to be Y_2O_3.

The large voids distributed in F82H-mod are expected, while it is somewhat surprising to see similar voids in ODS alloys PM2000 and 14YW. It has been identified that sample F82H-mod exhibits large voids when irradiated to 380 appm He / 9 dpa at 500°C [10]. The ODS alloys, however, have a distinct microstructure from RAFM. It is anticipated that the high density of nano-oxides in ODS alloys should trap He in numerous subcritical size bubbles. The appearance of voids in the ODS alloys examined here may have three causes. First of all, the total available sites for He bubble nucleation is limited, which sets a threshold of He concentration that the alloy can contain. A He concentration above that limit may turn some He bubbles into voids. This limit is expected to be higher for ODS alloys than that for RAFM steels.

The other factor, which may be responsible for the void formation in the samples examined in this study, is related to secondary phases. It is clear in sample PM2000 (Fig. 1a) that large bubbles are associated with particles. These particles were identified to be a Y-rich amorphous phase. Similar void-particle association also exists in sample 14YW, as shown in Fig. 2a. Figs. 2(b) and 2(c) present the high-resolution lattice image and its Fast-Fourier-Transformation (FFT) of the particle. EDX cannot precisely measure the particle composition as the particle takes only about 5% of the excitation volume. However, the EDX quantification at the particle gives a Y concentration up to 3.1 wt.%, which is more than ten times higher than that in the bulk sample (0.25 wt.%). Further FFT identification confirms an Y_2O_3 phase. This is anticipated as other elements in this alloy (i.e., Fe, Cr, and W) have a much lower affinity for O than Y. The third reason is that the PM2000 and 4YW are not the same as the ODS variant, that we call nanostructured ferritic alloys (NFA), since the former contain fewer and coarser oxides of different character than the $Y_2Ti_2O_7$ complex oxide that are dominant for the latter class of ferritic stainless steels. These results are important since they demonstrate that the size, number density and character of the nanofeatures and secondary phases play a key role in irradiation tolerance. The existence of good and bad phases has been previously observed in austenitic stainless steels and is discussed in Reference 11.

In sample 14YW, regions with enhanced void formation were identified. The voids appear to be associated with secondary phases. One example is shown in Fig. 3. The phase shown in Fig. 3 was identified as a Cr-rich phase, and its selected-area diffraction pattern (SADP) was indexed to be Cr_5O_{12}. It should be noted that all the phase identification in this study should be considered preliminary as it is only based on one or two diffraction patterns. It is not uncommon that one pattern can be indexed to be multiple phases. Unambiguous phase identification will be conducted by examining more than one SADPs at different tilt orientations.

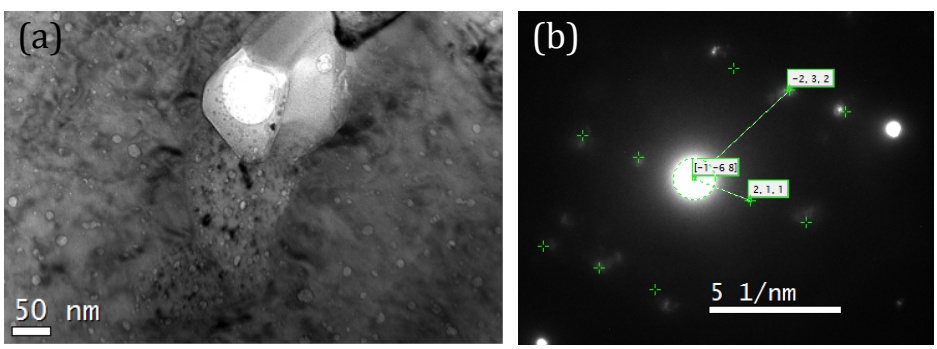

Fig. 3. (a) Bright-field TEM image of a Cr-rich secondary phase with large voids and bubbles, (b) SADP of the Cr-rich phase, which can be indexed to be Cr_5O_{12}. The SADP was overlapped with simulated diffraction patterns of Cr_5O_{12} phase under [-1 -6 8] zone axis.

Micrographs showing the dislocation loops seen in each alloy are shown in Fig. 4, and the measured loop size and density are summarized in Table 3. Note that only loops bigger than 4 nm were counted in this study. For each field of view, multiple micrographs at different two-beam conditions near the <100> zone axis are acquired, and a representative one is shown in Fig. 4. The diffraction vectors used to excite the loops are drawn in the micrograph. The rotation angle of the microscope is zero, indicating that the crystal orientation in the diffraction pattern and that in the micrograph are the same. Under the <100> zone axis, <100>{100} loops

exhibit edge-on double-line contrast perpendicular to <100> directions, while ½<111>{111} loops exhibit elliptical shapes with the major axis perpendicular to the <110> direction. Other types of dislocation loops were not observed, which is consistent with previous reports [9, 12]. The details of the method used for dislocation loop analysis can be found elsewhere [12].

Some interesting preliminary conclusions are obtained from this study. First, the high density of dislocation loops observed, and associated total line length, are much greater than expected for irradiations at 500°C. For example, in our previous study, the dislocation loop density of RAFM alloys irradiated to 9 dpa at 500°C with 380 appm He is much lower [13]. The loop density may increase at the higher dose, but this is inconsistent with the saturation of hardening at lower temperatures and the generally complete absence of hardening at higher temperatures around 500°C in ferritic alloys. The possible impact of high He levels on loop evolution remains to be determined. Secondly, a much higher density of <100>{100} than ½<111>{111} loops was found. This observation is consistent with other studies on RAFM/ODS alloys irradiated at high temperatures [12]. The different loop-density has been attributed to the higher mobility of ½<111>{111} loops, which might migrate to sinks such as grain boundaries, interfaces, and line dislocations. The <100>{100} loops, on the other hand, are less mobile and grow to form bigger loops. Although it has been reported that the <100>{100} loops at 500°C also have a significant mobility [14], the results from this study suggest otherwise. Lastly, the loops in PM2000 (30 nm for <100> loops) are larger than the two other alloys (16 nm and 19 nm). Note, that these observations are also preliminary and subject to future verification.

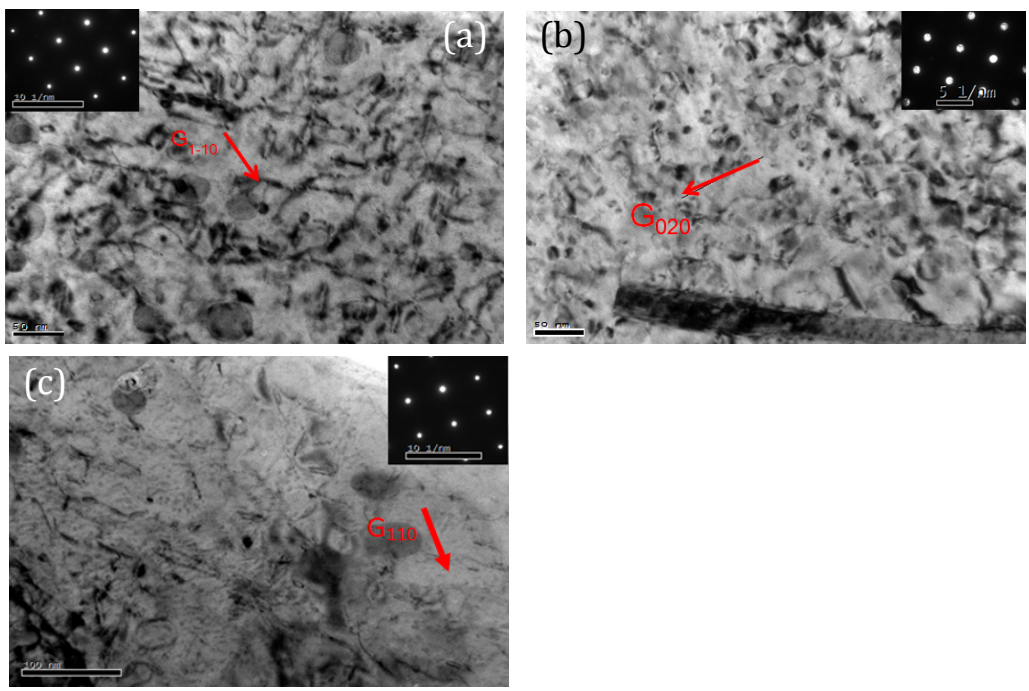

Fig. 4. TEM micrographs showing dislocation loops of samples (a) PM2000, (b)14YW, and (c) F82H-mod.

REFERENCES

[1] G. R. Odette, M. J. Alinger, and B. D. Wirth, *Annu. Rev. Mater. Res.* **38** (2008) 471.

[2] R. J. Kurtz, A. Alamo, E. Lucon, Q. Huang, S. Jitsukawa, A. Kimura, R. L. Klueh, G. R. Odette, C. Petersen, M. A. Sokolov, P. Spätig, and J. W. Rensman, *J. Nucl. Mater.* **386-388** (2009) 411.

[3] N. Baluc, K. Abe, J.L. Boutard, V.M. Chernov, E. Diegele, S. Jitsukawa, A. Kimura, R.L. Klueh, A. Kohyama, R.J. Kurtz, R. Lässer, H. Matsui, A. MÖslang, T. Muroga, G.R. Odette, M.Q. Tran, B. van der Schaaf, Y. Wu, J. Yu, and S.J. Zinkle, Nucl. Fusion 47 (2007) S696.

[4] H. Ullmaier, *Nucl. Fusion.* 24 (1984) 1039.

[5] R. E. Stoller and G. R. Odette, *J. Nucl. Mater.* **131** (1985) 118.

[6] R. Schäeublin and Y. L. Chiu, *J. Nucl. Mater.* **362** (2007) 152.

[7] G. R. Odette, P. Miao, D. J. Edwards, T. Yamamoto, R. J. Kurtz, and H. Tanigawa, *J. Nucl. Mater.* **417** (2011) 1001.

[8] B. Yao, D. J. Edwards, R. J. Kurtz, G. R. Odette, and T. Yamamoto, *Fusion Reactor Materials Program* **51** (2011), 85.

[9] B. Yao, D. J. Edwards, and R. J. Kurtz, G. R. Odette, T. Yamamoto, "Maps of Dislocation Loops in Irradiated bcc Fe–Based Steels." To be submitted.

[10] T. Yamamoto, G. R. Odette, P. Miao, D. J. Edwards, and R. J. Kurtz, *Fusion Reactor Materials Program* **44** (2008) 44.

[11] Y. Dai, G. R. Odette, and T. Yamamoto in: Konings R. J. M., (ed.) *Comprehensive Nuclear Materials*, Vol. 1 (2012) pp. 141-193 Amsterdam: Elsevier.

[12] J. Chen, P. Jung, W. Hoffelner, and H. Ullmaier, *Acta Materialia* **56** (2007) 250.

[13] D. J. Edwards, R. J. Kurtz, G. R. Odette, and T. Yamamoto, *Fusion Reactor Materials Program* **47** (2009) 59.

[14] R. Bullough and R. C. Perrin, *Proc. Roy. Soc. Lond. A* **305** (1968) 541.